

# SOLAR CELL EFFICIENCY ANALYSIS AND DEFECT IDENTIFICATION USING THE CELLO - TECHNIQUE

J. Carstensen<sup>1</sup>, S. Mathijssen<sup>1</sup>, G. Popkirov<sup>2</sup>, and H. Föll<sup>1</sup>

<sup>1</sup>Chair for General Materials Science, Faculty of Engineering, Christian-Albrechts-University of Kiel, Kaiserstr. 2, 24143 Kiel, Germany, email: jc@tf.uni-kiel.de, Phone: (+49) 431 880 6181, Fax: (+49) 431 880 6178  
<sup>2</sup>Bulgarian Academy of Sciences, Central Laboratory for Solar Energy and New Energy Sources, Sofia, Bulgaria

**ABSTRACT:** The CELLO (solar CELI LOfcal characterization) technique is described shortly and methods to identify several types of local defects by combining maps measured at several points along the IV-characteristics are discussed for an example of a multicrystalline solar cell. From the current and voltage response at the working point of the solar cell the influence of defects on the solar cell efficiency can be analyzed in linear order. Since CELLO only needs the standard contacts for measuring currents and voltages it can be applied to nearly all kinds of solar cells.  
**Keywords:** Characterization, Multi-Crystalline, Solar Cell Efficiencies

## 1 CELLO MEASUREMENT TECHNIQUE

### 1.1 Introduction

The CELLO (solar CELI LOfcal characterization) technique allows to measure all parameters of the equivalent circuit of a solar cell (cf. Fig. 1) *locally* [1, 2]. The technique analyses the current and voltage response induced by local illumination with a modulated LASER beam on a globally illuminated solar cell. Using a very stable potentiostat/galvanostat, a four probe arrangement for the contact electrodes, and a Lock-in amplifier the linear response is measured at several points along the IV-characteristics of the solar cell as illustrated in Fig. 2. The amplitude and phase shift of the linear response are measured with a high lateral resolution ( $\sim 200 \mu\text{m}$ ), i.e.  $\sim 500.000$  pixel for a  $(100 \times 100) \text{mm}^2$  cell.

The influence of different defect types on current and voltage differs along the IV-characteristics. This allows to identify defect structures, either directly or by combining data measured at different points along the IV-characteristics. The amplitude data allows to obtain qualitative and often quantitative information about the distribution of diffusion length of minorities, shunts, serial resistance, and emitter quality.

### 1.2 Active compensation of ohmic losses

The solar cell is contacted in a four probe arrangement: two electrodes are used to measure voltages (reference electrodes) and two electrodes are used to apply a voltage resp. a current to the solar cell. The potentiostat compensates ohmic losses in the wiring by fixing the voltage measured by the reference electrodes. Thus only local ohmic losses from the LASER illuminated spot to the position of the reference electrode on the front grid (i.e.  $R_{ser}(x,y)$ ) are not compensated and therefore measurable. Using only one reference electrode on the front grid of a large solar cell leads to a very unsymmetrical distribution of serial resistances across the solar cell. Therefore the signal of up to four symmetrically positioned reference electrodes is electronically averaged and this signal is used for controlling and measuring the voltage in the CELLO setup. This approach satisfactorily stabilizes the working point for measuring CELLO maps along the IV-characteristics of a solar cell.

### 1.3 CELLO phase shift

Due to the active compensation of resistance losses, the CELLO short circuit current measurements differ somewhat from LBIC [3] results.

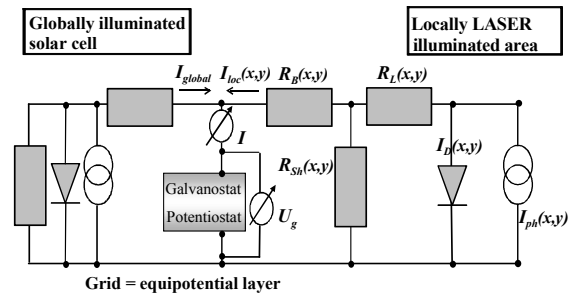


**Figure 1:** Simplified equivalent circuit of the CELLO system.

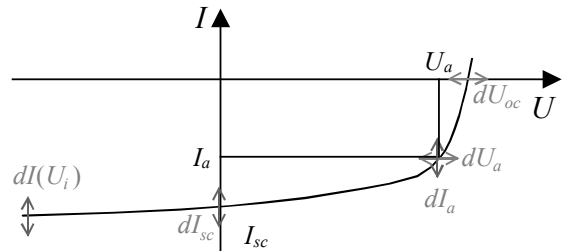


**Figure 2:** The five most common CELLO measurement modes along the IV-curve of a solar cell. The suffix “a” refers to the optimal working point of the cell.

For a pure current measurement like LBIC all resistances, including the contact resistance at the solar cell and the wire resistances, add up to a full resistance  $R$  which is responsible for a low pass behavior with a time constant  $\tau_{RC} = RC$ , where  $C$  is the capacitance, mainly caused by the pn-junction. With CELLO, however, only the local resistance losses of the solar cell  $R_{ser}(x,y)$  lead to a low pass behavior with a time constant  $\tau_{RC}(x,y) = R(x,y)C(x,y)$  where  $C(x,y)$  sums up all capacitances at the illuminated spot. The full time constant, responsible for the phase shift in the CELLO measurements, is  $\tau(x,y) = \tau_{lifetime}(x,y) + \tau_{RC}(x,y)$ , where  $\tau_{lifetime}(x,y)$  is the local lifetime of the minority carriers. Thus the CELLO phase shift contains qualitative information about the local capacity of the cell, and thus, e.g., of the local emitter quality, the doping concentration, and the back surface field. The phase shift information is supplementary to the amplitude information, and different effects in the amplitude maps can be understood using the phase shift information.

## 2 RESULTS AND DISCUSSION

### 2.1 Short circuit current

As an example for various defect structures that can be detected with CELLO, a 10 cm x 10 cm multicrystalline solar cell has been chosen. Fig. 3 shows a number of CELLO maps for this cell. The short circuit map  $dI_{sc}$  (Fig. 3a) shows the typical grain structure with a high recombination activity of the grain boundaries. The cell was fabricated from a wafer near the edge of a block, so the grains at the right side show a more columnar structure with grain boundaries nearly perpendicular to the edge of the cell. Around all four edges the recombination is slightly increased, following perfectly straight lines. This marks the areas without Al metallization at the backside. As a guide to the eye at the lower left edge in Fig. 3a, a part of this straight line is highlighted by a thick white line.

### 2.2 Open circuit voltage and serial resistance

The same structure is visible in several of the other CELLO maps as well. Fig. 3b shows the voltage response at open circuit condition  $dU_{oc}$ . Here the boundaries are regions with strongly reduced voltage response. In strong forward direction solar cells are dominated by the serial resistance losses. Following the procedure as described, e.g. in [4], from the  $dU_{oc}$  and  $dI_{sc}$  maps, and including the information of the global IV-characteristics, the serial resistance from the illuminated spot to one of the four reference electrodes can be calculated. The result is shown in Fig. 3d. Obviously the edge regions show an increased serial resistance due to the missing backside metallization near the edges. Additionally increased serial resistances exist around several grid fingers, which are marked by squares, and are easily identified as broken grid fingers, e.g. by optical microscope investigation.

### 2.3 Phase shift of short circuit current

The increased serial resistance cannot be the reason for the additional losses in the short circuit current near the edges of the solar cell since under short circuit condition the serial resistance is not relevant. For a qualitative understanding the phase shift of the short circuit current (Fig. 3c) can be used. As discussed in the previous section, the phase shift contains information on the lifetime. Therefore the grain boundaries with small lifetimes show a significantly smaller phase shift. Additionally the phase shift is sensitive to the local RC component. So a larger phase shift is expected in regions with larger serial resistances. This is true for the broken grid fingers. Although not easily visible in the gray scale maps (in contrast to color coded maps), the phase shift here is always larger than in the surrounding areas. But for the edge region of the solar cell it is vice versa. Here a smaller phase shift is found, although the serial resistance is larger. This can be explained by a systematically reduced capacitance in exactly the same region with an increased serial resistance, i.e. the missing of BSF charges and therefore BSF capacitances due to the missing metallization. So the missing BSF can be identified as the reason for the increased recombination around the edges of the solar cell.

The lack of a BSF is always related to the missing of the backside metallization near the edges of solar cells. But on more modern cell structures frequently no substantial additional serial resistance losses have been found with CELLO. This example shows that for a detailed understanding of solar cell efficiencies, a tech-

nique like CELLO is needed, which can identify various independent effects on key parameters of solar cells.

Another effect directly related to the local capacitance is the smaller phase shift at the right side of the solar cell. Here differences in the capacitance of the pn-junction become visible. The doping of the wafer is lower at the right side, which is typical for the regions near a block edge, leading to a smaller pn-junction capacitance.

### 2.4 Quantification of defect related efficiency losses

As illustrated above the best way to identify defects is the comparison of CELLO maps from different points along the IV-characteristics. To quantify the influence of defects on the solar cell efficiency mainly the current and voltage response at the working point of the solar cell (Fig. 3e and Fig. 3g) are taken, because only these maps show the correct influence of defects on current and voltage relevant for the solar cell efficiency. In these two maps all defects which have been identified are visible. Since the power  $P = I_a U_a$  depends on the product of current and voltage at the working point, the relative losses in power in linear order depend on the relative losses in current and voltage, i.e.

$$\frac{\Delta P}{P} = \frac{\Delta I_a}{I_a} + \frac{\Delta U_a}{U_a}. \quad (1)$$

One would expect that this relation holds as well for the averages  $\langle dI_a \rangle$  and  $\langle dU_a \rangle$  of the corresponding CELLO maps, but the correct relation is

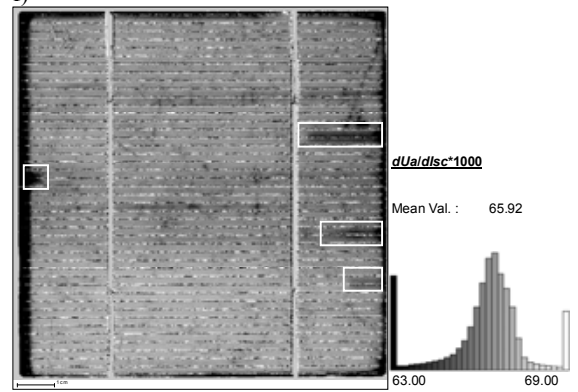
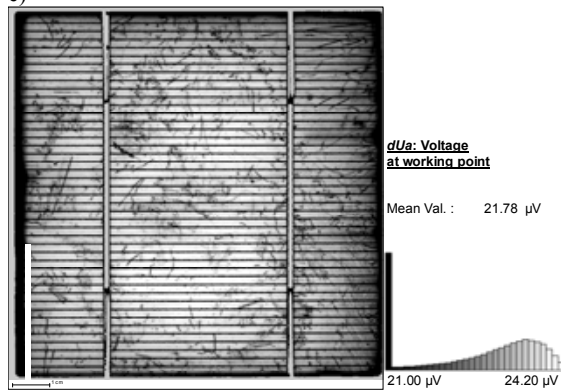
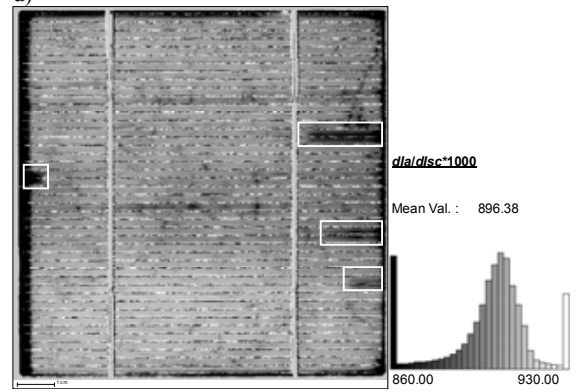
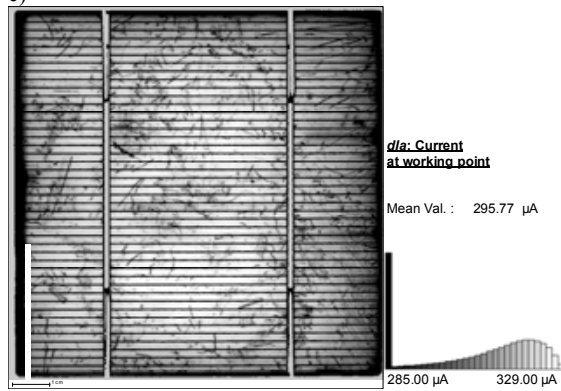
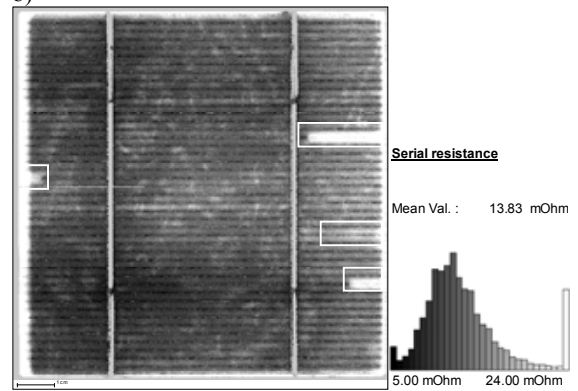
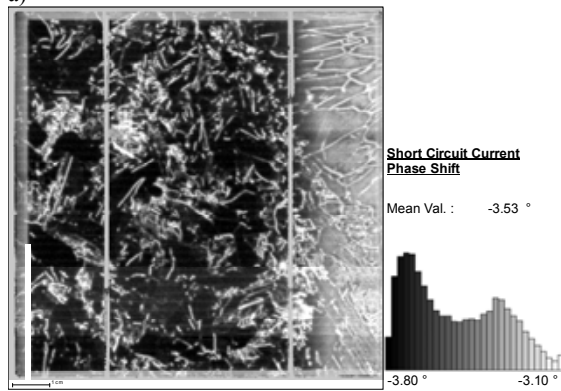
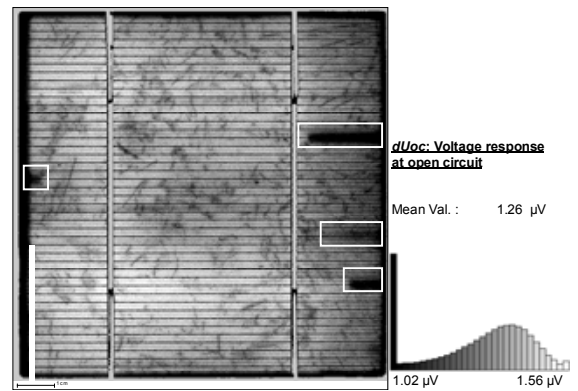
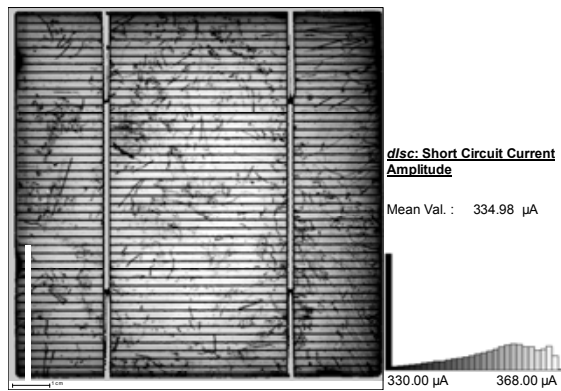
$$\frac{\Delta P}{P} = \frac{\Delta \langle dI_a \rangle}{\langle dI_a \rangle} + \frac{\Delta \left\langle \frac{dU_a}{dI_{sc}} \right\rangle}{\left\langle \frac{dU_a}{dI_{sc}} \right\rangle}, \quad (2)$$

i.e. not the local voltages should be summed up, but the corresponding (inverse) resistances. Fig. 3h shows the  $dU_a/dI_{sc}$  map. Since the grain structure is nearly invisible in this map, it is much easier to identify the process-induced defect structures. To decouple material-induced defect structures from bulk recombination for the current as well, the corresponding ratio  $dI_a/dI_{sc}$  is calculated in Fig. 3f. From the three maps in Fig. 3a, 3f, and 3h the linear losses in power can be calculated by

$$\frac{\Delta P}{P} = \frac{\Delta \langle dI_{sc} \rangle}{\langle dI_{sc} \rangle} + \frac{\Delta \left\langle \frac{dI_a}{dI_{sc}} \right\rangle}{\left\langle \frac{dI_a}{dI_{sc}} \right\rangle} + \frac{\Delta \left\langle \frac{dU_a}{dI_{sc}} \right\rangle}{\left\langle \frac{dU_a}{dI_{sc}} \right\rangle}. \quad (3)$$

For estimating e.g. the efficiency losses related to the broken grid fingers, the four dark areas marked by the squares can be graphically replaced by numbers from corresponding areas without broken grid fingers. Since these defects do not show up in the short circuit current, they only have to be replaced in Figs. 3f and 3h leading to a mean value of 896.88 for the relative current and 65.95 for the relative voltage and an improvement in the efficiency of only

$$\frac{\Delta P}{P} = \frac{0.5}{896.9} + \frac{0.03}{65.9} = 0.1\%.$$



g)  
**Figure 3:** CELLO maps for a 10 cm x 10 cm multicrystalline silicon solar cell. a) short circuit current  $dI_{sc}$  (amplitude); b) voltage at open circuit  $dU_{oc}$ ; c) phase shift of short circuit current; d) calculated serial resistance map; e) current response at working point of solar cell  $dI_a$ ; f) map of  $dI_a/dI_{sc} * 1000$ ; g) voltage at working point  $dU_a$ ; h) map of  $dU_a/dI_{sc} * 1000$ .

Although the grid fingers are clearly visible in nearly all images, their influence on the efficiency is very small. This example shows, how sensitive CELLO is to local defects.

As a second example, losses related to the missing backside metallization will be quantified. In this case the losses in the photo current have to be taken into account as well. Without the afflicted edge areas, the mean values increase to 337.6  $\mu\text{A}$  for the short circuit current, 903.8 for the relative current, and 66.44 for the relative voltage, leading to

$$\frac{\Delta P}{P} = \frac{2.6}{335} + \frac{6.8}{896.9} + \frac{0.54}{65.9} = 2.4\%$$

This is a much larger problem than the influence of broken grid fingers, but still an acceptable loss at the edge of a solar cell.

2.5 Shunt identification and CELLO results on other types of solar cells.

The mc-Si solar cell discussed above did not show significant shunts. Therefore the shunt detection mode was not discussed in that section. Due to lack of space, here it will only be mentioned, that for other cells, a comparison of the CELLO shunt detection mode with IR tomography [5] showed a good agreement, at least for ohmic shunts, and that shunts which have been identified by IR tomography as non-linear shunts, are visible in CELLO, e.g., in the serial resistance maps.

Since CELLO only needs the standard contacts for measuring currents and voltages, a number of thin-film solar cells, e.g. CIGS and  $\mu\text{cSi}$  cells, have been investigated with CELLO as well [6]. Especially the resistance maps for such solar cells showed very interesting structures, which were not visible in LBIC or in IR tomography (and are not easily obtained with other methods, e.g. CORESCAN [7]) CELLO with its full capability can thus be applied to nearly all kinds of solar cells. No other technique can provide a comparable wealth of information on thin film cells (usually covered with glass).

### 3 SUMMARY AND CONCLUSIONS

CELLO is a non-destructive method which allows to characterize nearly all local solar cell parameters qualitatively (Shunts, serial resistance, lifetime, BSF, pn-junction capacitance), and most of them quantitatively. This was demonstrated in this paper for a mc-Si solar cell. CELLO is applicable to nearly all types of solar cells. Since CELLO measures data sequentially, the measurement time is quite long for high spatial resolution ( $\approx 500000$  pixel per map). Typical scan rates are 100 pixel per second, but scan rates up to 300 pixels have already been demonstrated. Improvement in the hardware, especially an increased signal to noise ratio, will allow to increase the measurement speed further.

In addition to the amplitude, the phase shift is measured for each point. Since the phase shift contains independent information about the solar cell parameters, this nearly doubles the information measured per time. Up to now the phase shift information is just interpreted qualitatively; but the implementation of separately measured lifetimes (e.g. by an LBIC mode) will allow to separate the influence of the RC components and thus will enable CELLO to quantify local capacitances; providing quanti-

tative numbers for, e.g., BSF and pn-junction capacitance.

### 4 REFERENCES

- [1] J. Carstensen, G. Popkirov, J. Bahr, and H. Föll, in *Proceedings of the 16th European Photovoltaic Solar Energy Conference*, VD3.35, Glasgow (2000).
- [2] J. Carstensen, G. Popkirov, J. Bahr, and H. Föll, *Solar Energy Materials & Solar Cells* **76**, 599 (2003).
- [3] C. Donolato, *Solid. State Electron.* , 68 (1982).
- [4] S. Mathijssen, J. Carstensen, G. Popkirov, and H. Föll, in *Proceedings of the 20th European Photovoltaic Solar Energy Conference*, 1AV.2.41, Barcelona (2005).
- [5] M. Langenkamp and O. Breitenstein, *Solar Energy Materials & Solar Cells* **72**, 433 (2002).
- [6] S. Mathijssen, J. Carstensen, H. Föll, G. Voorwinden, and H. Stiebig, in *Proceedings 2005 MRS Spring Meeting*, in press, San Francisco (2005).
- [7] A.S.H. van der Heide, A. Schönecker, G.P. Wyers, and W.C. Sinke, in *Proceedings of the 16th European Photovoltaic Solar Energy Conference*, VA1.60, Glasgow (2000).